Sādhanā (2022) 47:150
https://doi.org/10.1007/s12046-022-01926-y
© Indian Academy of Sciences

Analysis of EDM machining parameters for keyway on Ti-6Al-4V alloy and modelling by artificial neural network and regression analysis methods

RAMAZAN ÇAKIROĞLU

Vocational School of Technical Sciences, Gazi University, Ankara, Turkey
e-mail: rcakiroglu@gazi.edu.tr

MS received 16 October 2021; revised 26 January 2022; accepted 19 May 2022

Abstract. Keyed joints are one of the most widely used methods of motion and power transmission. The high functionality and reliability of the joining elements depend on their resistance to the thermo-mechanical stresses that occur during operation and their high precision manufacturing. In this context, a widespread analysis of keyway opening and machining parameters (discharge current, pulse on time and pulse off time) was carried out according to DIN 6885 standard by a die-sinking electrical discharge machine on Ti-4Al-6V alloy with poor machinability. First, the effects of processing parameters on material removal rate (MRR), tool wear rate (TWR) and surface roughness (SR) were investigated by EDM experiments in a kerosene environment. It was seen that the discharge current and the pulse on time have a significant effect on the processing outputs MRR, TWR and SR. In addition, the processed surface and subsurface formations were comprehensively evaluated with SEM and EDS analyses. By reason of the low thermal conductivity of Ti6Al4V, it has been determined that the depth of the heat affected zone reaches 60 μm. In the second stage, mathematical models were developed for the prediction of processing outputs using artificial neural network (ANN) and regression analysis (RA) methods. When these two methods were compared, it was determined that the modelling results with ANN were closer to the experimental results.

Keywords. EDM; Ti-6Al-4V alloy; Material removal rate; Tool wear rate; Surface roughness; ANN; Regression analysis.

1. Introduction

Key and keyways are the important methods used to fix power transmission elements such as gear wheels and belts to the rotating shaft [1]. The fact that the key and keyways are made of suitable materials and high precision to withstand the torque force that must be transmitted in power transmission, and the stresses that will occur in sudden start and stop situations of rotational movement is a situation that increases the functionality and reliability of the system. The dimensions of the key and keyway are usually determined by the diameter of the shaft. However, it is a serious disadvantage that the key and the keyway are not made in the desired dimensions [2]. By creating the amount of assembly space outside the key and keyway tolerance values, a continuous impact will occur between the key and keyway during the operation of the system and will cause the machine element to malfunction. Therefore, it is important that the keyway is made of high-strength material and made in the desired dimensions. Titanium alloys are widely used in vibrating parts operating at high temperatures and speeds. It comes to the fore in various engineering fields such as defence, aerospace, engine turbine, vehicle manufacturing and biomedical. The use of titanium alloys in such wide areas is due to their strength-to-weight ratio, excellent mechanical and physical properties, toughness, excellent resistance to corrosion and high yield stress [3]. In addition to these superior properties, titanium alloys also have some disadvantages. Since it has low thermal conductivity, adhesions occur between the cutting tool and the workpiece in traditional machining methods. In addition, high chemical reactivity that damages the cutting tool occurs at high temperatures during machining. Considering these disadvantages, it is extremely difficult to process titanium alloys with conventional methods [4].

Unlike conventional machining techniques, electrical discharge machining (EDM) is widely used in the machining of hard and conductive materials, regardless of the mechanical properties of the metal [5]. EDM is an unusual machining technique that applies a high-frequency electrical discharge between a conductive material and an electrode in a dielectric fluid, thereby melting small parts from metallic materials and removing chips by evaporation [6]. In this machining method, the resultant values such as

Published online: 26 July 2022

metal removal rate (MRR), tool wear rate (TWR), surface roughness (SR) and dimensional accuracy depend entirely on the input parameters (discharge current, pulse on time, pulse off time, voltage). The use of ideal machining parameters is very important in obtaining high metal removal rates and desired dimensions with the best surface quality without forming any white film or heat affected zone. The fact that the machined parts will be used in important places such as keyways, which provide movement and power transfer by operating at high temperature and speed, increases the importance of processing parameters.

Various studies are continuing to examine the EDM performance of the titanium alloy. Verma *et al* investigated the effects of submerged electrical discharge machining parameters on MRR, TWR and SR in the machining of titanium alloy using copper electrodes. Pulse on time, pulse off time, fluid press and voltage parameters were used as processing parameters in the experiments. In their study, they obtained higher material removal rate using high voltage, high pulse duration and medium dielectric flow pressure. Increasing the pulse on time caused an increase in microcracks on the machined surfaces. In addition, dielectric flow pressure played an important role in increasing the material removal rate. It has been observed that low dielectric flow pressure is insufficient to remove debris, and forms recast layers [7]. Klocke *et al* compared the effect of polarity in the machining of Ti-6Al-4V titanium and 42CrMo4 iron alloy by die-sinking EDM [8]. Bhaumik *et al* evaluated the effect of different tool materials such as copper, brass and zinc on MRR and TWR during the EDM performance of Ti grade 6. They achieved higher MRR with brass and zinc tools compared to copper tools. However, the copper electrode performed better in tool wear [9]. Perumal *et al* optimized the effects of EDM processing parameters on Ti-6Al-4V titanium alloy with Taguchi approach. In their experiments, they investigated the effects on MRR and TWR by using three different diameters of copper tool and current, spark on time, voltage parameters. Maximum MRR was obtained with 6 mm diameter copper tool with Ip 20 A, 60 V servo voltage and 100 µs spark, while low tool wear was obtained at 10 mm diameter, 10 Ip current, 80 V voltage, 50 µs spark on time parameters [10]. Singh *et al* tried different washing methods to improve the washing action during the EDM process. They used perforated and non-perforated copper tools. They observed that washing processes using compressed argon gas from perforated tools had a positive effect on MRR and TWR in general [11].

In the machining of titanium alloys with EDM, low metal removal rate, high tool wear occurs, and at the same time, heat affected zones are formed together with the layers formed on the machined surfaces [13]. The problems experienced in removing the residues that occur in places such as holes and keyways in EDM machining directly affect the use of the produced workpieces. For this reason, it provides great advantages to be able to accurately predict the results by developing mathematical models based on processing parameters. By using the processing parameters and the MRR, TWR and SR values obtained as a result of these parameters, estimated values were tried to be obtained by ANN and RA methods [14–16].

As a result of the literature review, a study similar to the keyway opening with EDM on a high-temperature material that is difficult to machine, such as Ti-6Al-4V titanium alloy, was not found. This study focused on creating different geometries such as channels, hollows, grooves, etc. with EDM on this alloy and comprehensive analysis of machining outputs according to machining parameters. For this purpose, EDM experiments were carried out in different machining parameters in order to open a keyway on Ti-6Al-4V alloy with 14 mm diameter in accordance with DIN 6885 standard. End of the experiments, MRR, TWR and SR were evaluated based on different discharge current, pulse on time and pulse off time. SEM and EDS analyses were also conducted to assessment the variations on the workpiece and copper electrode surfaces. In addition, the experimental results were compared with the MRR, TWR and SR results obtained using ANN and RA method. The usability of the models developed by this comparison was also investigated. Thus, experimental data will be revealed that will be useful when creating different geometries with EDM in industrial applications for high temperature materials that are difficult to process.

2. Experimental and modelling processes

2.1 *Workpiece and tool (electrode) design*

One of the main purposes of this study is to open a keyway into Ti-4Al-6V titanium alloy in die-sinking EDM. Key and keyway dimensions are determined by standards based on only one parameter, the shaft diameter. Ti-4Al-6V titanium alloy with a diameter of 14 mm was used as the workpiece material. For the specified diameter according to DIN 6885 standard was determined according to the keyway dimensions as width (b) 5 mm, depth (h) 5 mm, shaft keyway depth (t_1) 3 mm and length (L) 20 mm. 99.5% pure copper, which is widely used in EDM applications, was preferred as the electrode material.

2.2 *Determination of processing parameters*

Experiments were carried out on Furkan compact a Z-NC die-sinking EDM machine. In order to process the Ti-4Al-6V titanium alloy with EDM with the desired quality, in the minimum time and with the least tool wear, many preliminary experiments were carried out by trying different machining parameters. Some workpiece and tool

images obtained as a result of preliminary experiments are given in figure 1. As seen in figure 1, it is very important to use ideal machining conditions in the processing of Ti-4Al-6V titanium alloy with EDM. Large coves in the tool, debris and burns occurred in the workpiece in the preliminary experiments carried out at high discharge current and low impact times. The high energy density passing through the plasma channel at high current caused the tool to wear [17].

Increasing the pulse on time causes the plasma channels to expand in the radial direction and decrease the intensity of the current [18]. For this reason, Ti-6Al-4V titanium alloy could be machined at high impact time without the formation of coves in the tool and debris in the workpiece. In the preliminary experiments, it was seen that the correct adjustment of the washing pressure and method is very important in cleaning the residues. In addition, pulling the tool back from the point where the workpiece started to work provided more effective washing during cleaning the debris [19].

As a result of the preliminary experiments and literature review, three different discharge currents (I_p), three different pulse on time (T_{on}) and two different pulse off times (T_{off}) were determined as variable parameters. In Table 1, the levels of variable processing parameters and the parameters kept constant are given. The experimental design created according to the determined processing parameters is given in Table 2.

Table 1. Machining parameters.

Process parameters / Variable parameters	Levels		
	1	2	3
Discharge current, A	9	12.5	15
Pulse on time, µs	150	200	250
Pulse off time, µs	100	120	–
Fixed parameters			
Flushing pressure, kgf/cm^2	0.4		
Retract distance (RD), mm	4.5		
Tool working time until retract, s	1.5		
Peak voltage of pulse generator, V	60		
Workpiece material	Ti-6Al-4V		
Workpiece polarity	Negative		
Tool electrode material	Copper		
Tool polarity	Positive		
Dielectric fluid	BELONE EDM F		

2.3 *Obtaining processing outputs*

In order to obtain MRR and TWR values, the weights of the workpiece and tool were measured with a precision balance of 0.001 g before and after each machining. MRR and TWR values were obtained using equations (1) and (2), respectively [6].

$$MRR = (w_b - w_a)/(\rho x t)\left(mm^3/mm\right) \quad (1)$$

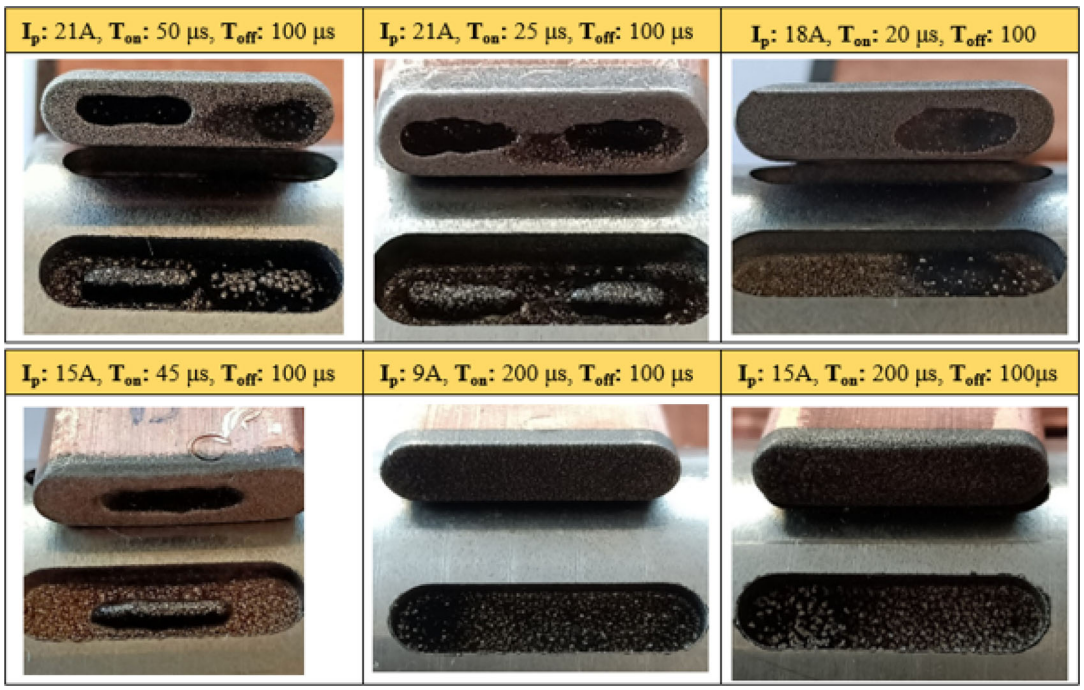

Figure 1. Workpiece and tool images obtained in preliminary experiments.

Table 2. Experiment design.

Exp. No.	Discharge current I_p	Pulse on time T_{on}	Pulse off time T_{off}
1.	9	150	100
2.	9	200	100
3.	9	250	100
4.	12.5	150	100
5.	12.5	200	100
6.	12.5	250	100
7.	15	150	100
8.	15	200	100
9.	15	250	100
10.	9	150	120
11.	9	200	120
12.	9	250	120
13.	12.5	150	120
14.	12.5	200	120
15.	12.5	250	120
16.	15	150	120
17.	15	200	120
18.	15	250	120

$$TWR = (w_b - w_a)/(\rho x t)\left(mm^3/mm\right) \quad (2)$$

Where w_b is the weight in gram before process, w_a is the weight in grams after processing, ρ is the density in g/mm^3, t is the processing time in minutes.

Mitutoyo device was used to measure surface roughness values. Surface roughness measurements were carried out after cutting the ends of the samples on a wire-cut EDM. Four different measurement values were taken from each sample and the average was calculated. Surface roughness values were used as $\lambda c = 0.8$ mm and $\lambda s = 2.5$ mm in the measurement conditions. In addition, SEM images and EDS analysis were conducted to made surface topography and metallurgical analysis of the machined surfaces. Figure 2 shows the experimental set up and workflow.

2.4 *Artificial neural network (ANN)*

ANN is a mathematical modelling widely used in the production of new data by learning, remembering, and using the information it learns when encountering data that it has never seen [20]. In this modelling, the training of the available data is done first. However, a certain part of the available data is not used in training to test the accuracy of the model. "Phytica" software was used to train the data and determine the most suitable network structure. In this study, three input layers (I_p, T_{on}, T_{off}), two hidden layers and three output layers (MRR, TWR, SR) feedback 3-5-5-3 network structure shown in figure 3 are used. In ANN, each connection between layers and neurons is defined as a weight vector (w) [21, 22]. Equations used in the Levenberg-Marquardt algorithm for this network structure are given below [21]:

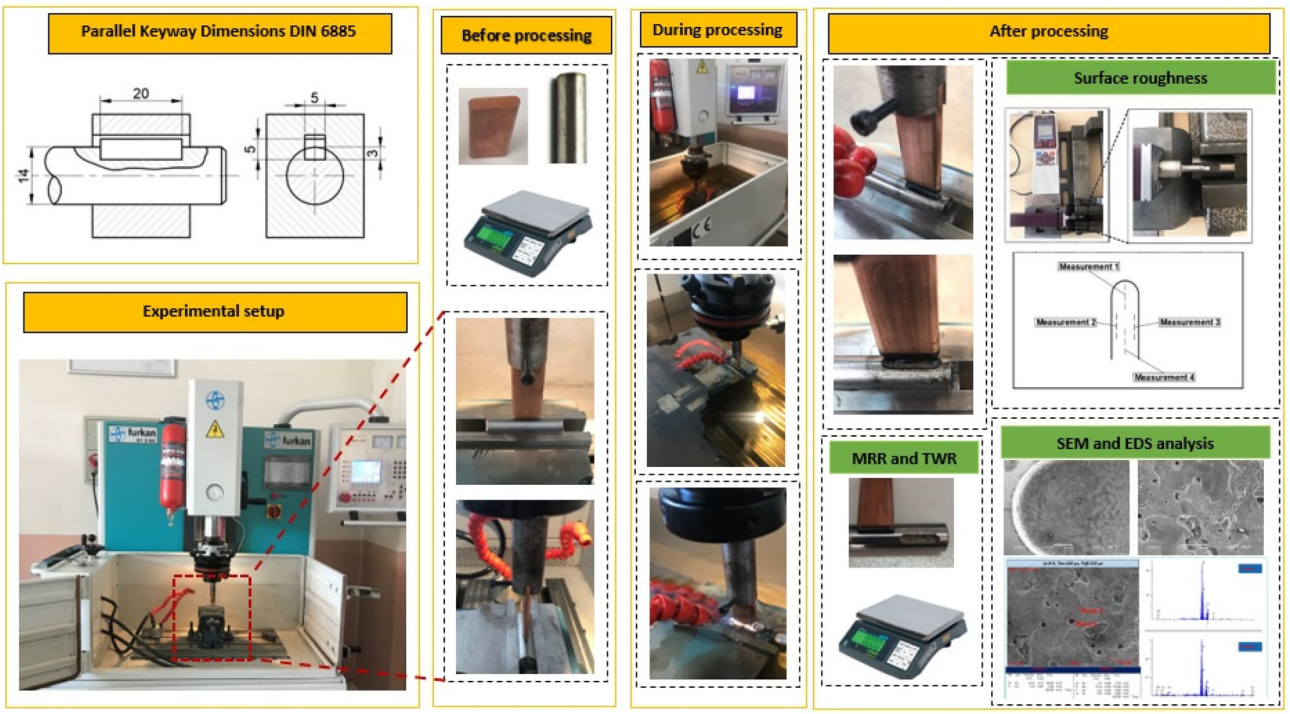

Figure 2. Experiment set up and workflow.

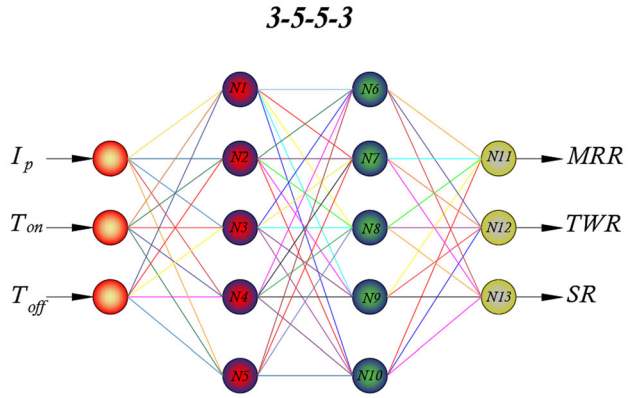

Figure 3. Network structure.

Hidden layer calculations;

$$Net_i = \sum x_i w_{ij}$$
$$y_i = f(Net_i) \quad (3)$$

Output layer calculations;

$$Net_k = \sum y_i w_{jk}$$
$$O_k = f(Net_k) \quad (4)$$

Here, x_i represents the input data, y_i represents the results from layer one, and O_k represents the second layer results. Transfer function.

The Fermi activation function was used to calculate both the hidden and output layers;

$$F_i = \left(1 + e^{-4(NET_i - 0.5)}\right)^{-1} \quad (5)$$

According to the determined network structure, the first layer weight values (j:1, 2, 3, 4, 5) and the second layer weight values (k:6, 7, 8, 9, 10) used in the estimation of MRR, TWR and SR values, and these layers Equations for $NET_{j(1-5)}$ and $NET_{k(6-10)}$ are given in Table 3. Fermi transfer functions for MRR, TWR and SR values are given in Equations (6), (7) and (8).

$$MRR = 1 + e^{-4*}(1.142645 * F_6 - 2.082553 * F_7 + 0.405395 * F_8 + 0.306453 * F_9 + 1.463076 * F_{10}) \quad (6)$$

$$TWR = 1 + e^{-4*}(1.110801 * F_6 - 0.811925 * F_7 + 1.73445 * F_8 - 1.43415 * F_9 + 0.284736 * F_{10}) \quad (7)$$

$$SR = 1 + e^{-4*}(-1.47311 * F_6 - 0.417066 * F_7 + 0.036373 * F_8 + 0.754891 * F_9 + 1.187372 * F_{10}) \quad (8)$$

2.5 *Regression analysis (RA)*

RA, different processing parameters (I_p, T_{on}, T_{off}) with outcome parameters (MRR, TWR and SR) was used to estimate the association between. A certain part of the available data has been kept separate to test the accuracy of

Table 3. Weights among layers for MRR, TWR and SR.

$NET_{j(1-5))} = w_{1j} * I_p + w_{2j} * T_{on} + w_{3j} * T_{off}$

j	*w1j*	*w2j*	*w3j*
Weights values between input and first hidden layers			
1	− 3.005299	2.346679	− 0.438041
2	5.867479	− 3.66935	− 1.76266
3	0.615318	0.071454	0.208378
4	0.393194	1.231715	0.160808
5	− 1.905345	− 0.858755	1.618952

$NET_{k(6-10)} = w_{1k} * F_1 + w_{2k} * F_2 + w_{3k} * F_3 + w_{4k} * F_4 + w_{5k} * F_5$

k	*W1k*	*W2k*	*W3k*	*w4j*	*w5j*
Weights values between first and second hidden layers					
6	0.049161	0.527045	− 0.449353	− 0.51568	0.443242
7	− 2.166971	− 2.553698	0.510502	0.315985	0.476942
8	− 1.803245	− 1.989637	3.384884	1.020086	− 2.791524
9	− 1.772434	− 2.803288	1.781711	2.759057	− 0.993356
10	− 2.592335	− 0.482145	0.197758	0.738577	− 1.176272

the model. In this study, a mathematical model was created by using the main factors (I_p, T_{on}, T_{off}). The regression coefficients in the created model were obtained with the help of Minitab statistical software. Estimation models for MRR, TWR and SR are given in equations (9), (10) and (11), respectively.

$$MRR = -0.00172 + 0.000317 * I_p + 0.000009 * T_{on} - 0.000001 * T_{off} \quad (9)$$

$$TWR = -0.00108 + 0.000171 * I_p - 0.000003 * T_{on} - 0.000004 * T_{off} \quad (10)$$

$$SR = 0.11 + 0.167 * I_p + 0.0177 * T_{on} - 0.00081 * T_{off} \quad (11)$$

2.6 *Statistical analysis*

Since the ANN and RA methods were carried out in two stages as training and testing, statistical analysis was performed to determine the amount of deviation (error) between the estimated value and the actual value, and the accuracy of the methods was checked. In this statistical analysis, absolute percent change (R^2), statistical error amount (RMSE) and mean percent error (MAPE) were evaluated. The highest values of R^2 and the lowest values of RMS and MAPE are the values in which the ANN and RA model have the highest performance [23]. These values were determined with the help of the following equations [20]:

$$R^2 = 1 - \left(\frac{\sum_{i=1}^{N} (t_i - o_i)^2}{\sum_{i=1}^{N} o_i^2} \right) \quad (12)$$

$$RMSE = \left(\frac{\sum_{i=1}^{N} |t_i - o_i|^2}{N} \right)^{1/2} \quad (13)$$

$$MAPE = \frac{1}{N} \sum_{i=1}^{N} \left(\left| \frac{t_i - o_i}{o_i} \right| \right) \quad (14)$$

here "t" is the target value, "o" is the output value and "N" is the number of experiments.

3. Result and discussion

3.1 *Surface structure*

SR values obtained in EDM processes are among the important output parameters. This value is expected to be low and this expectation increases the usability of the obtained workpieces. As a result of the experiments, the lowest SR value was obtained at 9A discharge current, 150 µs pulse on time and 120 µs pulse off time, while the highest SR value was obtained as 4.746 µm and 7.192 µm at 15A discharge current, 250 µs pulse on time and 120 µs pulse off time, respectively. At the highest T_{on} (250 µs) and highest T_{off} (120 µs) values, when the discharge current was increased from 9 A to 15 A, the SR value increased by approximately 23%. The SR values obtained depending on the processing parameters are presented in figures 4 and 5.

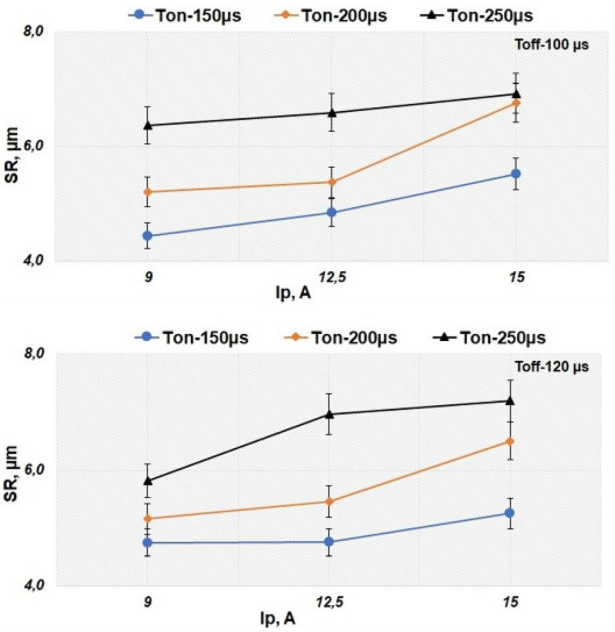

Figure 4. Effect of I_p on SR.

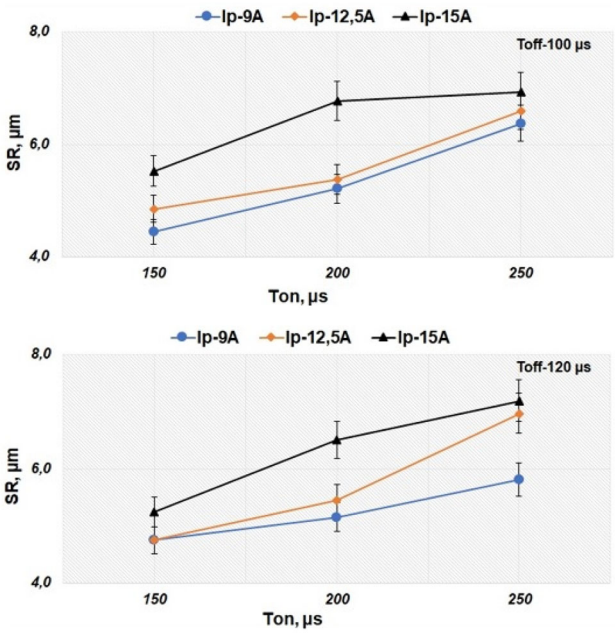

Figure 5. Effect of T_{on} on SR.

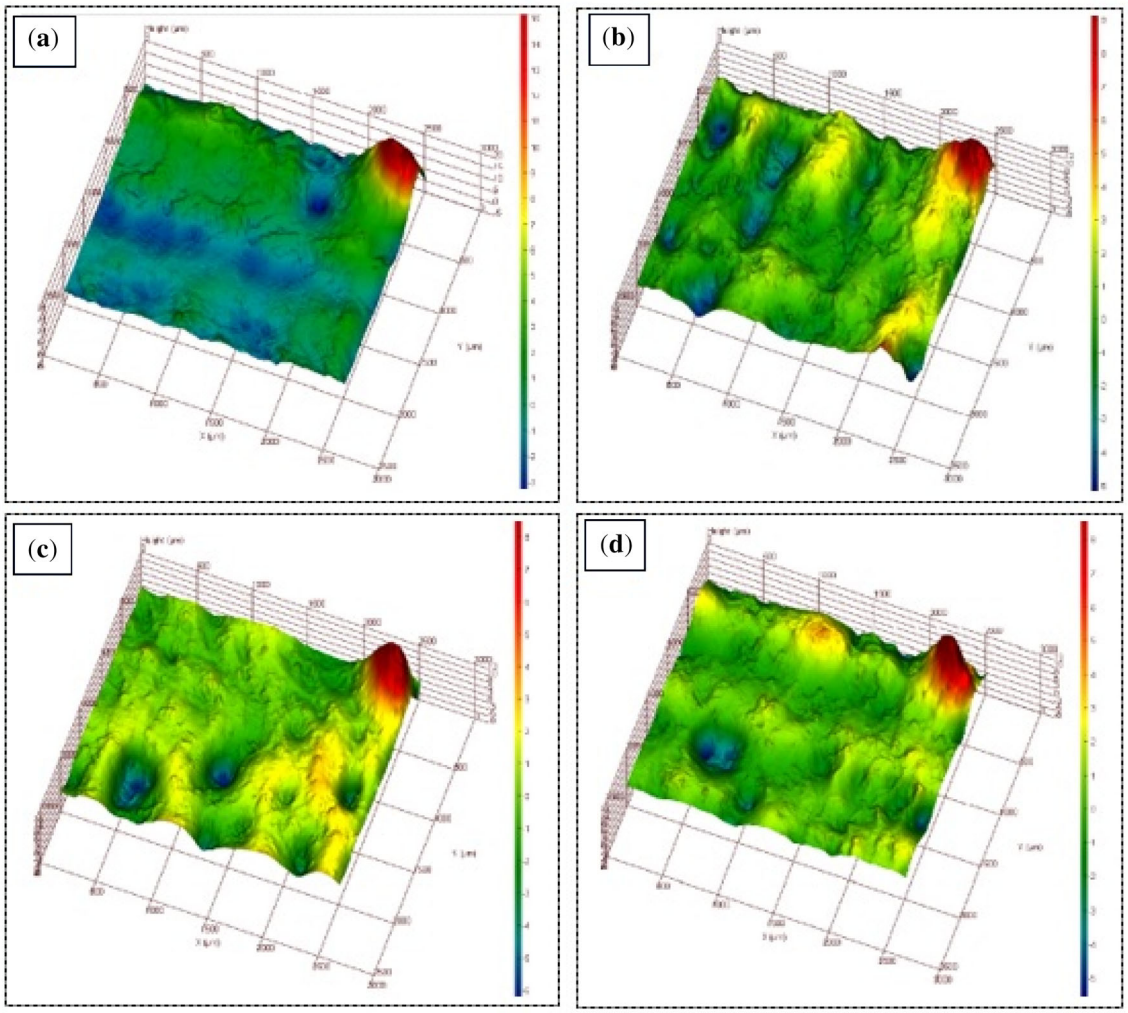

Figure 6. 3D surface topography. (**a**) Ip:9 A, Ton:150 µs, Toff:100 µs, (**b**) Ip:15 A, Ton:250 µs, Toff:100 µs, (**c**) Ip:9 A, Ton:150 µs, Toff:120 µs, (**d**) Ip:15 A, Ton:250 µs, Toff:120 µs.

When figures 4 and 5 are examined, the increases in SR values due to the increase in I_p values are clearly seen. It is known that SR values increase with the increase of I_p values [24–26]. This situation is explained by the increase in spark intensities with the increase in discharge current and the formation of deeper craters on the workpiece surface by the sparks with increasing intensity. These deep craters also cause increased SR results.

In the machined surface analysis, surfaces processed in four different parameters were considered. The surfaces obtained at the lowest and highest discharge current (9 A, 15 A) and pulse on time (150 µs, 250 µs) in pulse off time (100 µs, 120 µs) were compared. Figure 6 shows the 3D visualization of the machined surfaces. Figure 6(a) shows that the machined surface has a relatively homogeneous structure. Figure 6(b) shows the formation of more irregular structures consisting of peaks and valleys. The increase in I_p and T_{on} values has been an important factor in the deterioration of the homogeneous structure on the surface. With the increase in the density of the I_p and T_{on} parameters, the transfer of more intense thermal energy to the workpiece caused point melting and evaporation. Thus, deeper and wider craters are formed on the workpiece surface, resulting in an increase in the surface roughness value. The high thermal deformation caused by the increase in tone caused a significant increase in the depth and width of the crater formed on the surface and thus an increase in the SR value. However, the SR values did not show a parallel trend with the increase in the T_{off}. As T_{off} increased, the falling time of the spark changed at each current value. With the increase in the T_{on}, the workpiece surface was exposed to heat for a longer time and the amount of melting increased gradually. As a result, this caused an increase in the SR value by forming multi-directional irregular and randomly distributed deeper craters on the treated surface as stated by Ramasawmy and Blunt [27]. When figures 6(c-d) are examined, it is seen that a crater formation has occurred, which supports the above-

Table 4. Experimental and prediction results.

	Experimental			ANN			Ra		
Exp. No.	MRR	TWR	SR	MRR	TWR	SR	MRR	TWR	SR
*1.	0.002528	0.000423	4.442	0.002929	0.000646	4.949879	0.002383	0.000409	4.349
2.	0.002885	0.000372	5.207	0.002859	0.000438	5.229806	0.002833	0.000259	5.234
3.	0.003266	0.000318	6.374	0.003255	0.000383	6.371581	0.003283	0.000109	6.119
4.	0.003413	0.000881	4.850	0.003409	0.000925	4.835722	0.0034925	0.0010075	4.9335
5.	0.003846	0.000769	5.376	0.003872	0.000839	5.397278	0.0039425	0.0008575	5.8185
6.	0.004341	0.000736	6.595	0.004306	0.000806	6.590902	0.0043925	0.0007075	6.7035
*7.	0.004041	0.001878	5.524	0.003746	0.001817	4.971832	0.004285	0.001435	5.351
8.	0.004865	0.001396	6.772	0.004941	0.001422	6.775628	0.004735	0.001285	6.236
9.	0.005161	0.001124	6.929	0.005026	0.001177	6.989088	0.005185	0.001135	7.121
10.	0.002340	0.000381	4.746	0.002349	0.000431	4.782974	0.002363	0.000489	4.3652
11.	0.002992	0.000399	5.152	0.002997	0.000427	5.169953	0.002813	0.000339	5.2502
12.	0.003146	0.000330	5.813	0.003131	0.000386	5.861327	0.003263	0.000189	6.1352
13.	0.003386	0.000909	4.750	0.003363	0.000939	4.802794	0.0034725	0.0010875	4.9497
*14.	0.003945	0.000761	5.448	0.003752	0.000625	6.02354	0.0039225	0.0009375	5.8347
15.	0.004342	0.000714	6.968	0.004192	0.000753	6.943682	0.0043725	0.0007875	6.7197
16.	0.004298	0.002000	5.247	0.004324	0.001971	5.288515	0.004265	0.001515	5.3672
*17.	0.004774	0.001403	6.504	0.005035	0.001203	7.007964	0.004715	0.001365	6.2522
18.	0.005160	0.001119	7.192	0.005132	0.001158	7.158023	0.005165	0.001215	7.1372

* Excluded for testing

mentioned result. On the other hand, by increasing the T_{off} despite the increase in I_p, shallower craters were formed on the workpiece surface when no further machining was performed [28]. Average SR values taken from four different regions of the machined surface are given in Table 4.

SEM images of the treated ground surfaces at 250 X magnification are given in figure 7. It is clearly seen that the density of cracks, craters and voids varies according to the processing parameters. In figure 7(a), it is observed that no voids and cracks have formed on the machined surfaces, while in figure 10(b) it has been observed that microcracks and voids have formed. A similar situation is seen in figures 7(c) and figure 7(d). I_p was the main factor affecting crack and crater formations [7]. Increasing T_{on} time at the same I_p value caused the volume of molten crater to increase on the workpiece surface and the recast layer, of most of the molten metal in the craters [29]. This recast layer process occurs in the T_{off} process. It was observed that the density of cracks and voids in the craters formed with increasing T_{off} time increased. Layer thicknesses occurred on the side surfaces of the machined parts as well as the ground surface.

The reason for the formation of surface cracks; the tensile stresses caused by the shrinkage of the molten material during the cooling of the workpiece surface after sparks exceed the final tensile stress of the material in the white layer [30]. In addition, as it can be clearly seen in figure 7, microcracks, voids and surface unevenness increased with the increase of I_p value. In general, with increasing current in EDM machining, the density and power of the plasma channel created between the tool and the electrode increases, which increases the spark power and discharge energy. Due to the higher discharge energy, a higher thermal gradient occurs on the machined surface, resulting in more microcracks and void formations. In summary, an increase in the current density applied to the workpiece leads to the formation of micro cracks and voids, which will adversely affect the integrity of the machined surface. Therefore, it is recommended to use low currents when machining workpieces subject to cyclic loads and fatigue to avoid or reduce these negative effects [31].

Figure 8 shows the SEM images obtained after metallographic polishing on the cross-section of the samples processed with die-sinking EDM to determine whether there is a heat affected zone in different machining parameters of the Ti-4Al-6V titanium alloy. It was clearly seen that there was heat affected zones in all four different processing parameters shown in figure 8. It can be seen that there is a direct correlation between the processing parameters and the thickness of the heat affected zone [32–34]. While the thickness of the heat affected zone was approximately 10 μm in the sample processed with I_p 9 A, T_{on} 150 μs and T_{off} 100 μs parameters, this depth reached approximately 60 μm in I_p 15 A, T_{on} 250 μs and T_{off} 120 μs parameters. The low thermal conductivity of Ti-6Al-4V and the efficient and accurate use of the dielectric fluid, which prevents the high heat generated during processing from penetrating deep into the workpiece, ensured the thickness of the heat affected zone to be less than 100 μm [35].

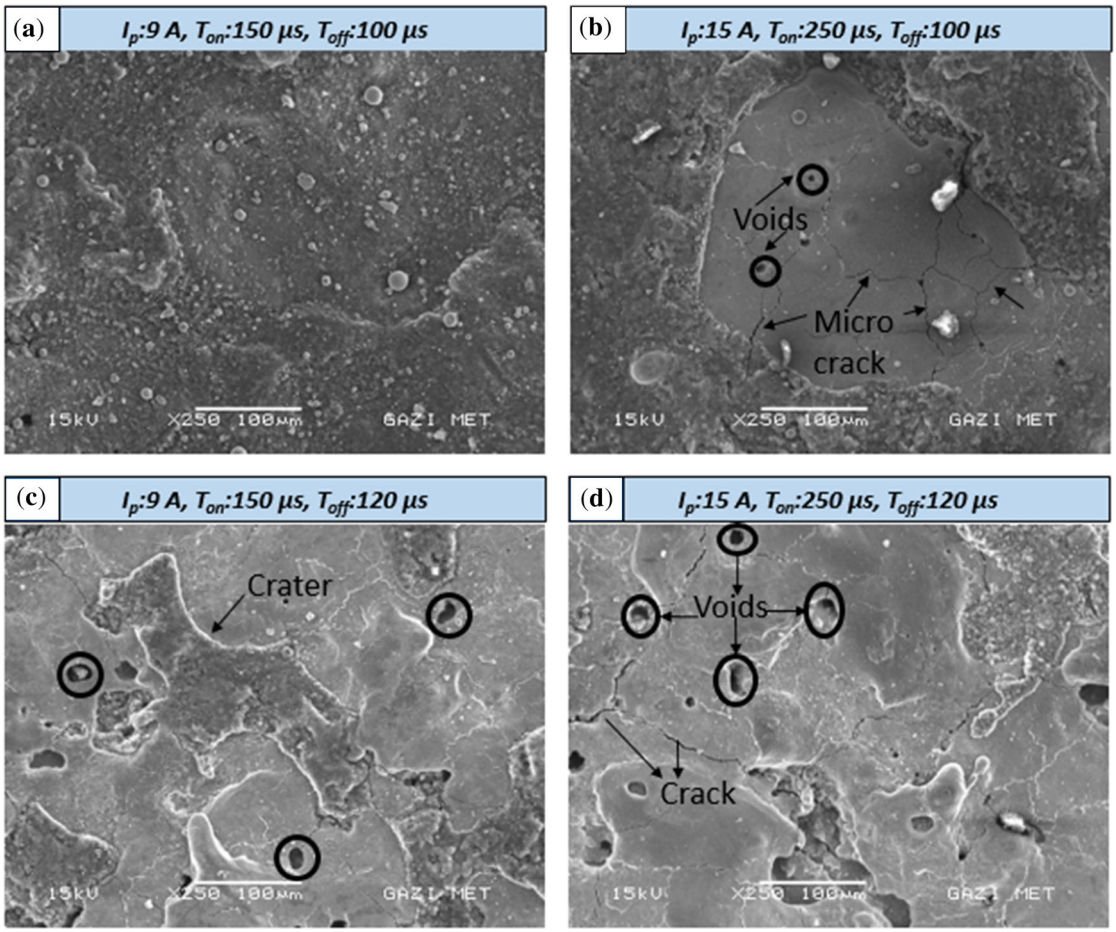

Figure 7. SEM images of the machined surface at 250X magnification.

Only 15% of the molten workpiece material is removed by the dielectric liquid [36]. The remaining materials are rapidly cooled by the dielectric and recast layer on the workpiece surface, forming a crater. The crater shape is not the same even when the processing conditions are constant on the same sample [37]. This is due to the various interactions of the resulting residues between the dielectric fluid and electric sparks. In addition, the dielectric sprayed between the workpiece and the electrode ensures that the residual parts are removed from the machining area and that the electric sparks fall evenly on the workpiece surface, allowing the wear on the tool surface to occur evenly [38, 39]. Therefore, better washing efficiency contributes to minimizing crater and void formation and ensuring surface integrity [40].

In figures 9 and figure 10, EDS analysis results are given from the machined surfaces of the 1st and 10th test samples, respectively, from the points 1 and 2 shown. As a result of both EDS analyses, the chemical compositions of the workpiece material Ti-6Al-4V alloy were observed. In figure 9, as a result of the analysis taken from the Point-2 point of the test sample 1 processed in I_p 9 A, T_{on} 150 µs and T_{off} 100 µs, the percentage weight of the aluminium material was higher, unlike the others. This is due to the inability to remove the residues from the processing area resulting from the melting of the workpiece material and the formation of the residues as a result of solidifying and sticking to the workpiece surface.

3.2 *Material removal rate*

As can be clearly seen in figures 11 and 12, increasing I_p and T_{on} parameters increased MRR [41]. The increase in I_p accelerated the melting and evaporation of the workpiece and the increase in the processing time with the increase in T_{on} significantly affected the MRR. The highest MRR value as a result of processing; while 15 A discharge current was obtained at 250 µs pulse on time and 120 µs pulse off time, the smallest MRR value was obtained as 0.005161 mm^3/min and 0.002340 mm^3/min at 9 A discharge current, 150 µs pulse on time and 120 µs pulse off time, respectively. At the highest T_{on} (250 µs) and lowest T_{off} (100 µs) values, when the discharge current was increased from 9 A to 15 A,

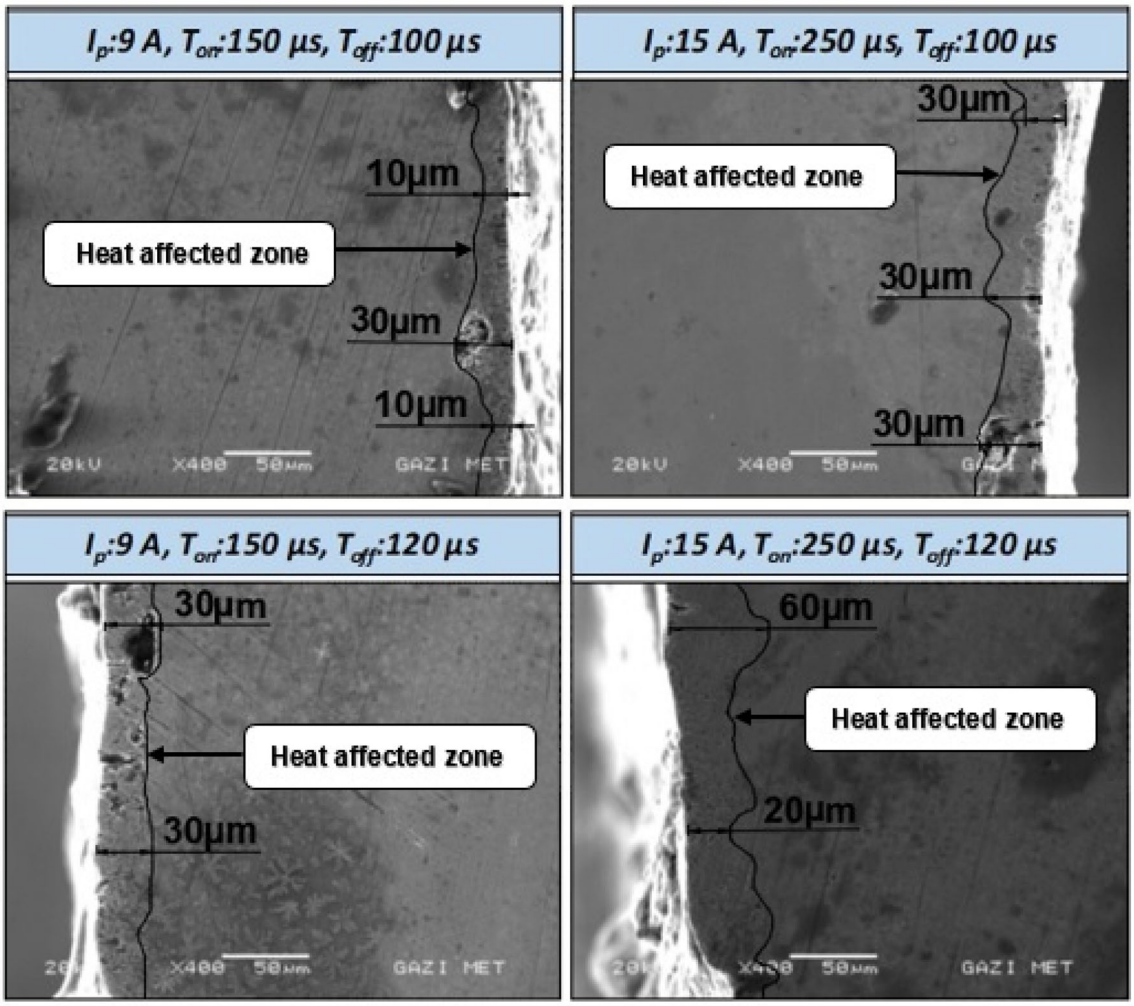

Figure 8. SEM views of machined surfaces after EDM.

the MRR value increased by approximately 36%. When compared in terms of tone value, an increase of approximately 22% was obtained when the pulse on time was increased from 150 µs to 250 µs at the highest I_p (15 A) and lowest T_{off} (100 µs) values. According to these processing parameters, it was seen that the T_{off} parameter did not have a significant effect on the MRR value [12]. For the same I_p and T_{on} parameters (I_p:15 A, T_{on}:150 µs), when the T_{off} parameter was changed from 100 µs to 120 µs, the difference was 5% at most. In addition, an important factor in obtaining high MRR values is the correct and appropriate pressure washing method. Especially as the processing depth increases, this factor becomes more important.

3.3 *Tool wear rate*

The effect of I_p on TWR is given in figure 13. TWR increased by 70% when increasing I_p from 9 A to 15 A. During the energy discharge, a plasma channel is formed between the tool and the workpiece, which affects the current conductor and heat generation. In this case, it is seen that high amount of melting and thermal erosion increase the temperature on the electrode surface and cause an increase in thermal deformation and wear of the tool [42, 43]. In figure 14, it is seen that TWR decreases as the T_{on} value increases. With the increase in ton, more carbon atoms were emitted and this formation formed a protective film that reduced tool wear [11, 44]. At the highest I_p (15 A) and lowest T_{off} (100 µs) values, the TWR was reduced by approximately 40% when the pulse on time was increased from 150 µs to 250 µs. In addition, the high-pressure spraying and the lift distance of the tool may have caused less melting of the tool and thus a decrease in TWR [45]. These reduction amounts are extremely important and will make a significant contribution to the applicability and economy of the system, especially in long-term processing. Therefore, it has been determined in the study that TWR values can be reduced by choosing the appropriate processing parameter and using the right cooling.

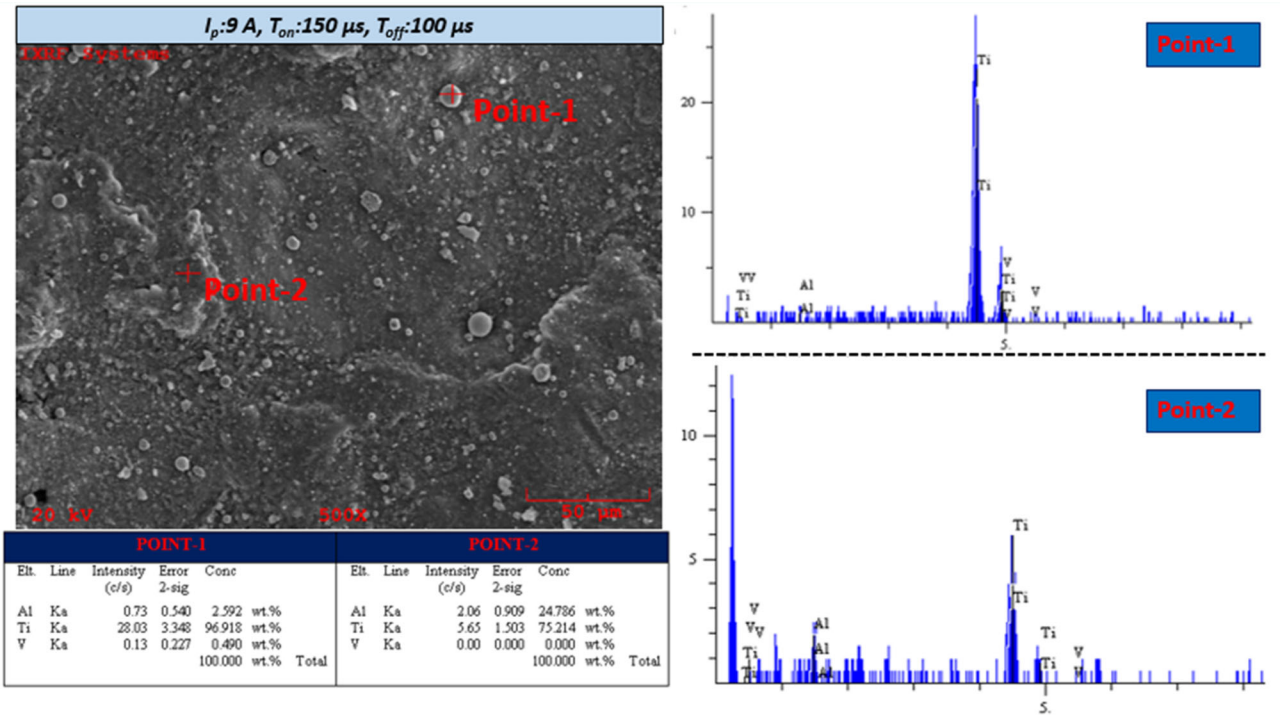

Figure 9. SEM and EDS images for the experiment conducted at I_p 9A, T_{on} 150µs, T_{off} 100µs.

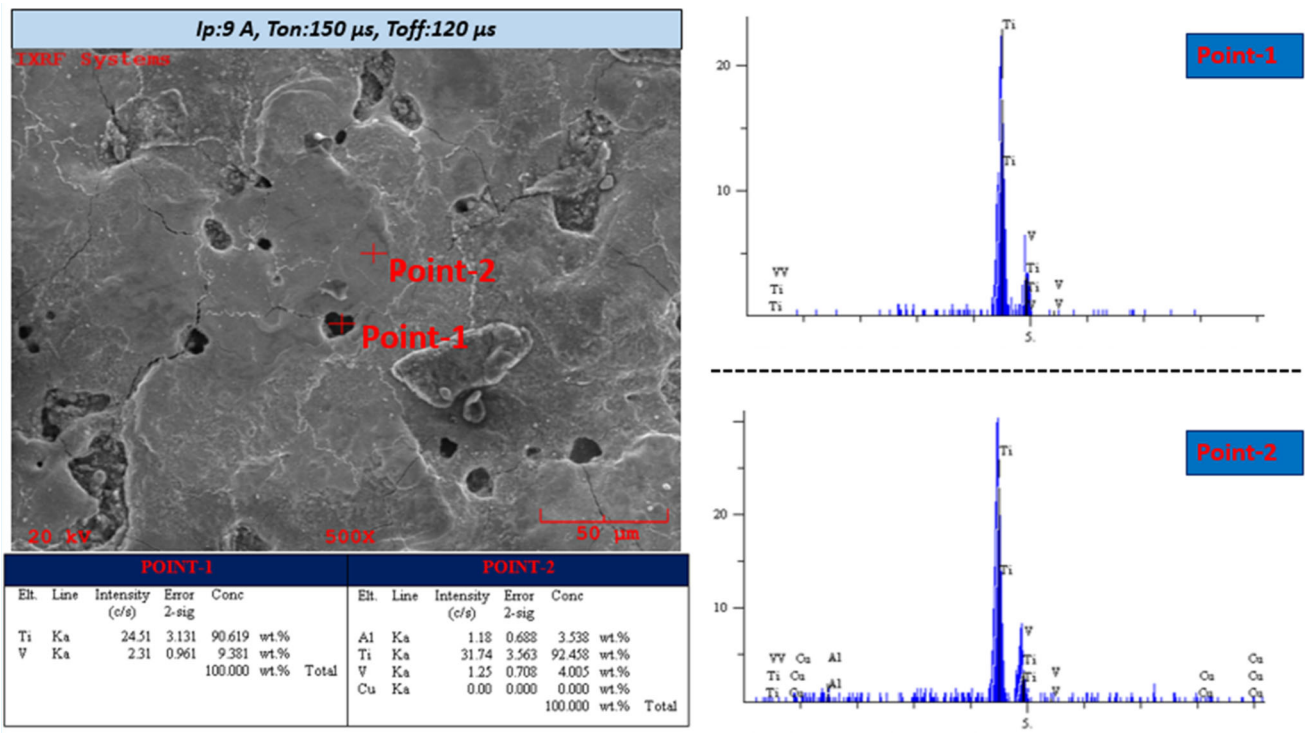

Figure 10. SEM and EDS images for the experiment conducted at I_p 9A, T_{on} 150µs, T_{off} 120µs.

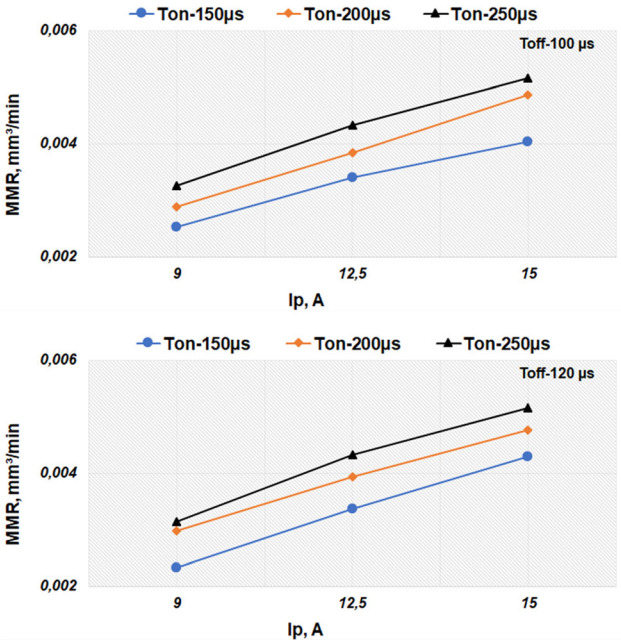

Figure 11. Effect of I_p on MRR.

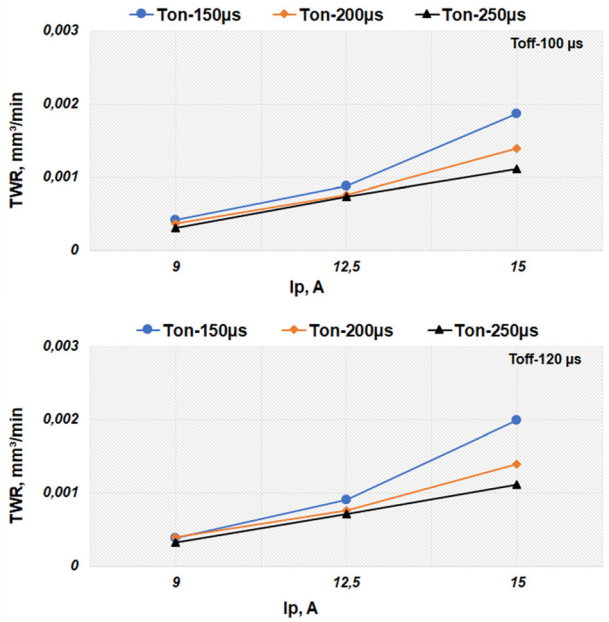

Figure 13. Effect of I_p on TWR.

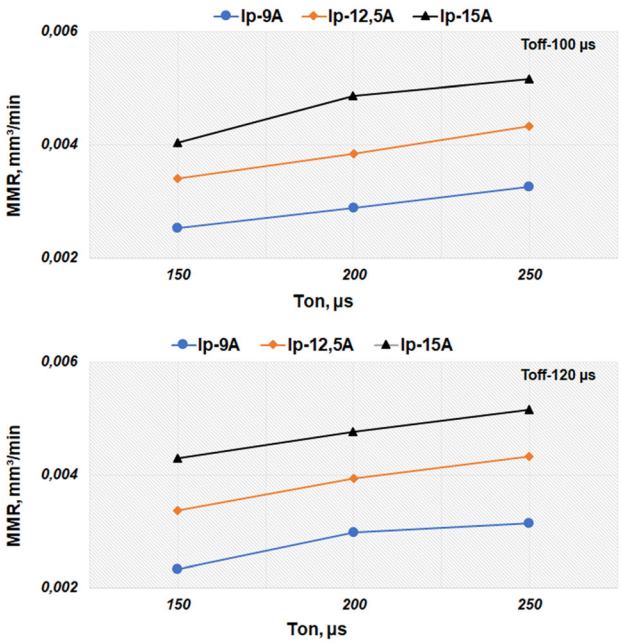

Figure 12. Effect of T_{on} on MRR.

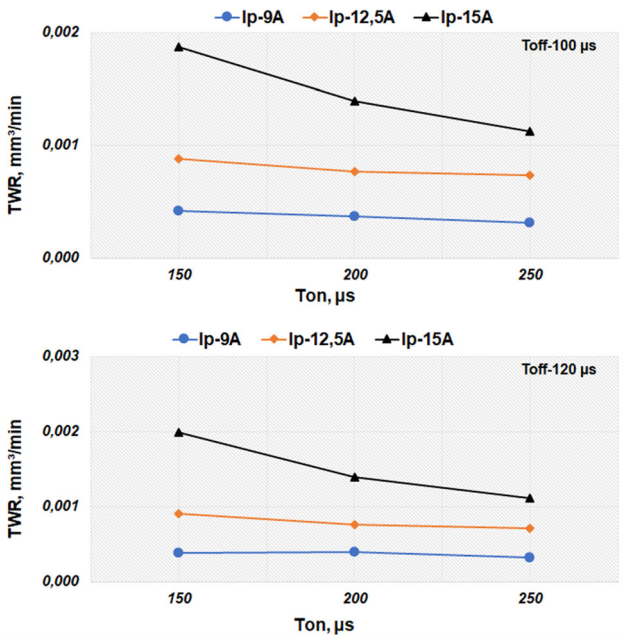

Figure 14. Effect of T_{on} on TWR.

3.4 *Modelling results*

In this study, it was aimed to evaluate the MRR, TWR, SR results by conducting experiments in different machining parameters in order to open a keyway in 14 mm diameter Ti-6Al-4V titanium alloy in accordance with DIN 6885 standard. Another aim of the study is to estimate the results of MRR, TWR and SR without the need for experimental studies in future studies by using the experimental results obtained. ANN and RA methods, which are widely used in the literature, were preferred to estimate the results and these two methods were compared. Experiment results and estimation results are given in Table 4. In the mathematical equations developed for the ANN and RA methods, 14 of the 18 experimental

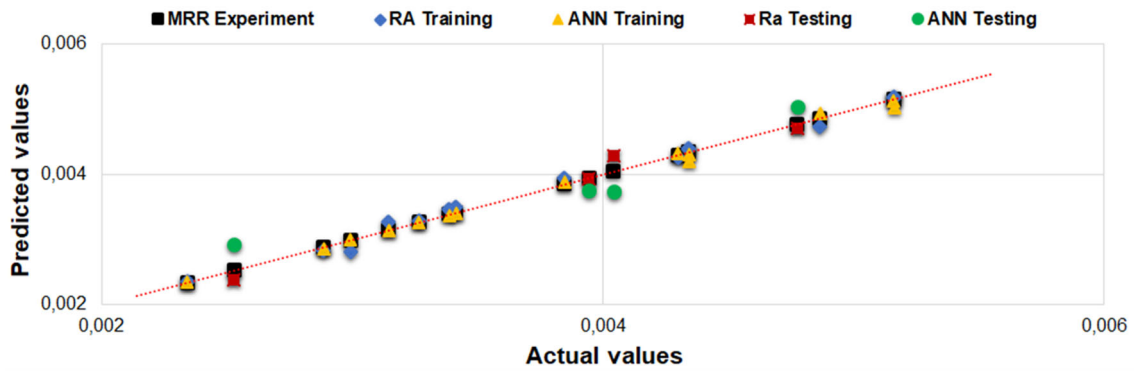

Figure 15. Comparison of MRR experimental results with ANN and RA results.



Figure 16. Comparison of TWR experimental results with ANN and RA results.

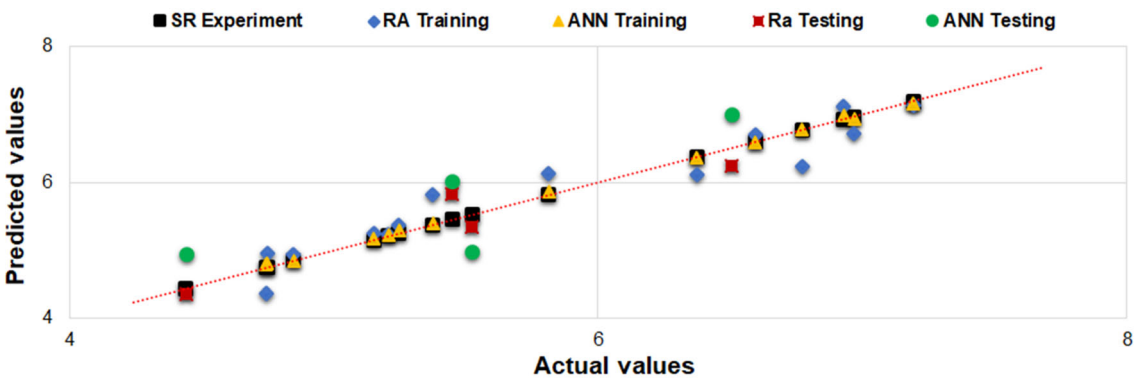

Figure 17. Comparison of MRR experimental results with ANN and RA results.

results were used for educational purposes, and 4 of them were reserved for checking the correctness of the equations. The equations used in estimating the results with the ANN and RA methods are given in Section (2). The comparison of the MRR, TWR and SR estimation results according to these equations with the actual experimental results are shown in figures 14, 15 and 16, respectively. As seen in figures 15, 16 and 17, it is seen that the ANN and RA estimated test results corresponding to the actual test results are close to each other.

The prediction performances of the ANN and RA models were determined by applying the coefficient of determination (R^2), mean squares of error (RMS) and mean absolute percent error (MAPE) methods given in Eqs. (6), (7) and (8). The performance values calculated for MRR, TWR and SR are shown in Table 5. As seen

Table 5. Statistical results of the MRR, TWR and SR.

	ANN			RA		
	RMSE	R^2	MAPE	RMSE	R^2	MAPE
MRR						
Training	0,020087	0,998888	0,281561	0,029333	0,997619	0,651501
Testing	0,10605	0,969626	5,809017	0,051868	0,992649	1,566297
TWR						
Training	0,011866	0,999167	2,17907	0,214796	0,873445	15,39948
Testing	0,100105	0,964613	15,52752	0,218392	0,762153	28,54538
SR						
Training	0,012878	0,999611	2,941859	0,146468	0,928369	7,35244
Testing	0,204038	0,91781	24,84214	0,140275	0,954487	11,82178

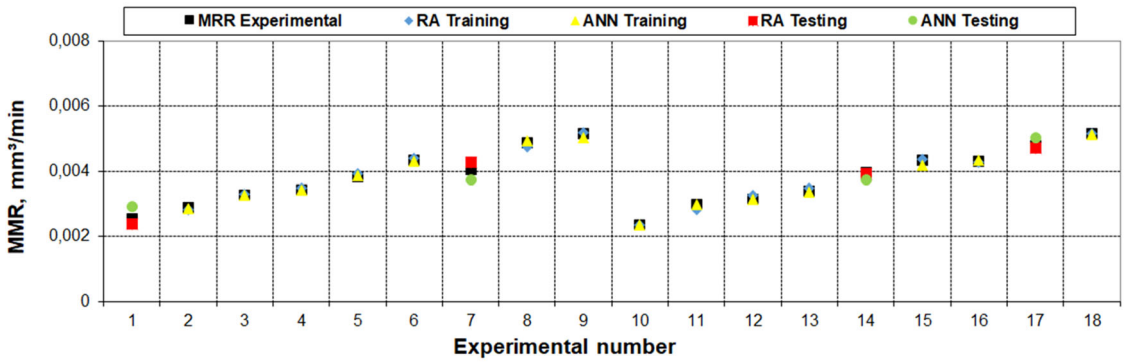

Figure 18. Comparison of experimental and predicted results for MRR.

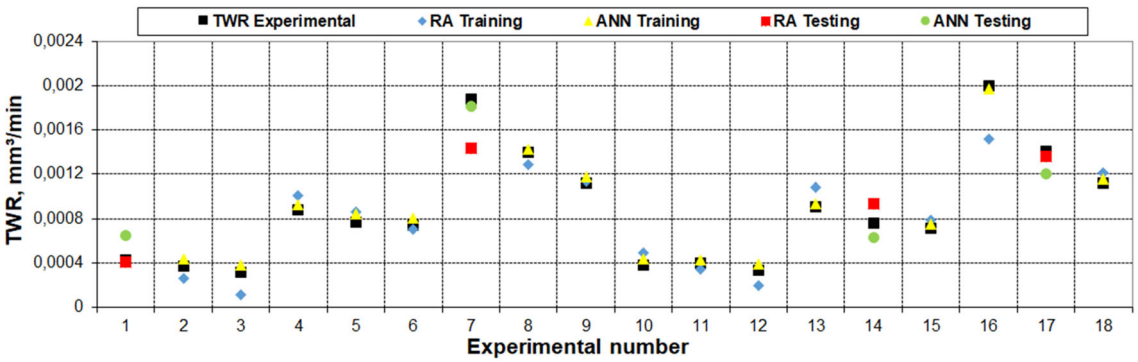

Figure 19. Comparison of experimental and predicted results for TWR.

in Table 5, the obtained results show that the ANN model developed for MRR, TWR and SR is close to accuracy.

The estimated results obtained with the ANN and RA equations showed good agreement with the experimental results. In addition, both the training results and the test results obtained as a result of the experimental study results and the ANN and RA equations are shown in figures 18, 19 and 20 respectively, for MRR, TWR and SR.

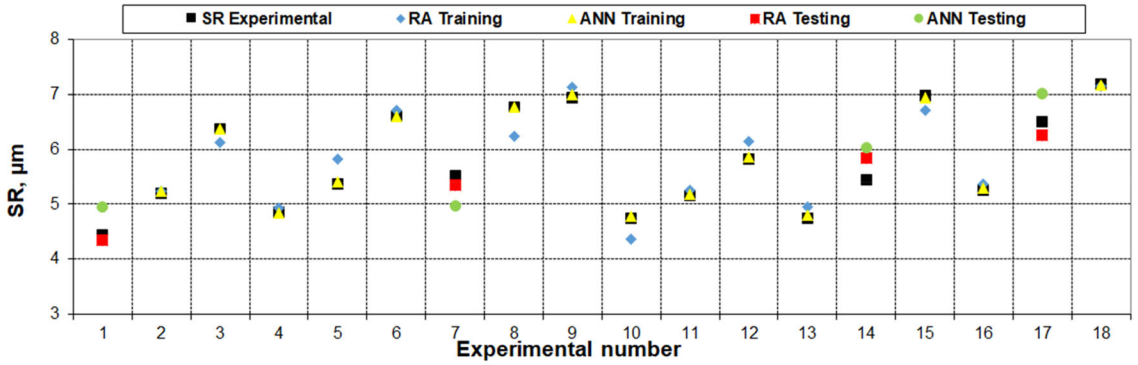

Figure 20. Comparison of experimental and predicted results for SR.

4. Conclusions

In this study, a comprehensive evaluation of the MRR, TWR and SR results obtained as a result of keyway cutting into Ti-4Al-6V titanium alloy with different machining parameters in die-sinking EDM was made. In addition, the MRR, TWR and SR test results obtained using ANN and RA methods were compared with the estimation results. The findings obtained as a result of the study are presented below:

- Increasing I_p and T_{on} parameters increased MRR. The highest MRR value; A discharge current of 15 A was obtained at a pulse on time of 250 µs and a pulse off time of 120 µs.
- It was observed that TWR increased as I_p increased, and TWR decreased as T_{on} value increased. At the highest I_p (15 A) and lowest T_{off} (100 µs) values, the TWR was reduced by approximately 40% when the pulse on time was increased from 150 µs to 250 µs.
- SR values increased with the increase of I_p. The lowest SR value (4.746 µm) was obtained in I_p 9 A, T_{on} 150 µs and T_{off} 120 µs parameters.
- The increase in I_p and T_{on} caused an increase in crack and crater formations. At the same time, it was observed that the density of cracks and voids in the craters formed with increasing T_{off} increased.
- Thanks to the low thermal conductivity of Ti6Al4V, the thickness of the heat affected zone is approximately 10 µm in the sample processed with I_p 9A, T_{on} 150 µs and T_{off} 100 µs parameters, and this depth is approximately 60 µm in I_p 15A, T_{on} 250 µs and T_{off} 120 µs parameters.
- ANN and RA methods were compared according to the results obtained. At the end of the study, it was determined that the ANN method gave more accurate results for this study than the prediction accuracy (R^2) in ANN and the prediction accuracy (R^2) in the RA model.

Abbreviations

MRR	Material removal rate
TWR	Tool wear rate
SR	Surface roughness
EDM	Electrical discharge machining
SEM	Scanning electron microscopy
EDS	Energy Dispersive Spectrometry
ANN	Artificial neural network
RA	Regression analysis
I_p	Discharge currents
T_{on}	Pulse on time
T_{off}	Pulse off times
RD	Retract distance
RMSE	Statistical error amount
MAPE	Mean percent error

References

[1] Sahu M K 2014 Optimization of the keyway design with consideration of effect of stress concentration on different materials. *Int. J. Eng. Res.* 3(5)

[2] Kishor H P and Raghu T 2014 Design analysis of a keyless coupling. *Int. J. Recent Res. Civ. Mech. Eng. (IJRRCME)* 1(1): 37–43

[3] Shokrani A, Dhokia V and Newman S T 2012 Environmentally conscious machining of difficult-to-machine materials with regard to cutting fluids. *Int. J. Mach. Tools Manuf.* 57: 83–101. https://doi.org/10.1016/j.ijmachtools.2012.02.002

[4] Su H H, Liu P, Fu Y C and Xu J H 2012 Tool life and surface integrity in high-speed milling of titanium alloy TA15 with PCD/PCBN tools. *Chin. J. Aeronaut.* 25(5): 784–790. https://doi.org/10.1016/S1000-9361(11)60445-7

[5] Sivakumar K, Kumar P M, Amarkarthik A, Jegadheeswaran S and Shanmugaprakash R 2021 Empirical modelling of material removal rate and surface roughness of OHNS steel using Cu-TiB2Tool in EDM. *Mater. Today Proc.* 45: 2725–2729. https://doi.org/10.1016/j.matpr.2020.11.597

[6] Çakıroğlu R and Günay M 2020 Comprehensive analysis of material removal rate, tool wear and surface roughness in electrical discharge turning of L2 tool steel. *J. Mater. Res. Technol.* 9(4): 7305–7317. https://doi.org/10.1016/j.jmrt.2020.04.060

[7] Verma V and Sajeevan R 2015 Multi process parameter optimization of diesinking EDM on titanium alloy (Ti6Al4 V) using Taguchi approach. *Mater. Today Proc.* 2(4–5): 2581–2587. https://doi.org/10.1016/j.matpr.2015.07.212

[8] Klocke F, Mohammadnejad M, Holsten M, Ehle L, Zeis M and Klink A 2018 A comparative study of polarity-related effects in single discharge EDM of titanium and iron alloys. *Proc. CIRP* 68: 52–57. https://doi.org/10.1016/j.procir.2017.12.021

[9] Bhaumik M and Maity K 2018 Effect of different tool materials during EDM performance of titanium grade 6 alloy. *Eng. Sci. Technol. Int. J.* 21(3): 507–516. https://doi.org/10.1016/j.jestch.2018.04.018

[10] Perumal A, Kailasanathan C, Stalin B, Rajkumar P R, Gangadharan T and Venkatesan G 2021 Evaluation of EDM process parameters on titanium alloy through Taguchi approach. *Mater. Today Proc.* 45: 2394–2400. https://doi.org/10.1016/j.matpr.2020.10.737

[11] Singh N K, Singh Y and Sharma A 2021 Experimental investigation of flushing approaches on EDM machinability during machining of titanium alloy. *Mater. Today Proc.* 38: 139–145. https://doi.org/10.1016/j.matpr.2020.06.165

[12] Pramanik A, Basak A K, Littlefair G, Debnath S, Prakash C, Singh M A and Singh R K 2020 Methods and variables in electrical discharge machining of titanium alloy—A review. *Heliyon* 6(12): 05554. https://doi.org/10.1016/j.heliyon.2020.e05554

[13] Ozkavak H V, Sofu M M, Duman B and Bacak S 2021 Estimating surface roughness for different EDM processing parameters on Inconel 718 using GEP and ANN. *CIRP J. Manuf. Sci. Technol.* 33: 306–314. https://doi.org/10.1016/j.cirpj.2021.04.007

[14] Singh N K, Singh Y, Kumar S and Sharma A 2020 Predictive analysis of surface roughness in EDM using semi-empirical, ANN and ANFIS techniques: A comparative study. *Mater. Today Proc.* 25: 735–741. https://doi.org/10.1016/j.matpr.2019.08.234

[15] Singh A K, Singhal D and Kumar R 2020 Machining of aluminium 7075 alloy using EDM process: An ANN validation. *Mater. Today Proc.* 26: 2839–2844. https://doi.org/10.1016/j.matpr.2020.02.591

[16] Debnath S, Rai R N and Sastry G R K 2018 A study of multiple regression analysis on die sinking EDM machining of ex-situ developed Al-45 cu-SiC composite. *Mater. Today Proc.* 5(2): 5195–5201. https://doi.org/10.1016/j.matpr.2017.12.101

[17] Schumacher B M 2004 After 60 years of EDM the discharge process remains still disputed. *J. Mater. Proc. Technol.* 149(1–3): 376–381. https://doi.org/10.1016/j.jmatprotec.2003.11.060

[18] Klocke F and König W 2007 Funkenerosives Abtragen (EDM). *Fertigungsverfahren 3: Abtragen. Generieren Lasermaterialbearbeitung.* 3–126

[19] Ayesta I, Izquierdo B, Sanchez J A, Ramos J M, Plaza S, Pombo I and Ortega N 2016 Optimum electrode path generation for EDM manufacturing of aerospace components. *Robot. Comput. Integr. Manuf.* 37: 273–281. https://doi.org/10.1016/j.rcim.2015.04.003

[20] Hanief M, Wani M F and Charoo M S 2017 Modeling and prediction of cutting forces during the turning of red brass (C23000) using ANN and regression analysis. *Eng. Sci. Technol. Int. J.* 20(3): 1220–1226. https://doi.org/10.1016/j.jestch.2016.10.019

[21] Çakıroğlu R, Yağmur S, Acır A and Şeker U 2017 Modelling of drill bit temperature and cutting force in drilling process using artificial neural networks. *Politeknik Dergisi.* 20(2): 333–340. https://doi.org/10.2339/2017.20.2333-340

[22] Altintas Y and Ber A A 2001 Manufacturing automation: metal cutting mechanics, machine tool vibrations, and CNC design. *Appl. Mech.* 54(5): B84–B84. https://doi.org/10.1115/1.1399383

[23] Şahin İ 2014 Yapay sinir ağları ile Al/Sic kompozit malzemenin yüzey pürüzlülüğünün tahmini. *Gazi Üniversitesi Mühendislik Mimarlık Fakültesi Dergisi*. 29(1). https://doi.org/10.17341/gummfd.82690

[24] Ahmed A 2016 Deposition and analysis of composite coating on aluminum using Ti–B4C powder metallurgy tools in EDM. *Mater. Manuf. Process.* 31(4): 467–474. https://doi.org/10.1080/10426914.2015.1025967

[25] Cogun C, Özerkan B and Karacay T 2006 An experimental investigation on the effect of powder mixed dielectric on machining performance in electric discharge machining. *Proc. Inst. Mech. Eng. Part B J. Eng. Manuf.* 220(7): 1035–1050. https://doi.org/10.1243/09544054JEM320

[26] Thakur A, Rao P S and Khan M Y 2021 Study and optimization of surface roughness parameter during electrical discharge machining of titanium alloy (Ti-6246). *Mater. Today Proc.* 44: 838–847. https://doi.org/10.1016/j.matpr.2020.10.785

[27] Ramasawmy H and Blunt L 2004 Effect of EDM process parameters on 3D surface topography. *J. Mater. Proc. Technol.* 148(2): 155–164

[28] Azhiri R B, Bideskan A S, Javidpour F and Tekiyeh R M 2019 Study on material removal rate, surface quality, and residual stress of AISI D2 tool steel in electrical discharge machining in presence of ultrasonic vibration effect. *Int. J. Adv. Manuf. Technol.* 101(9–12): 2849–2860. https://doi.org/10.1007/s00170-018-3023-5

[29] Ergün Z and Çoğun C 2006 Elektro erozyon ile işleme (EEİ) iş parçasi yüzey karakteristiklerinin deneysel incelenmesi. *Gazi Üniversitesi Mühendislik Mimarlık Fakültesi Dergisi* 21(3)

[30] Lee H T, Hsu F C and Tai T Y 2004 Study of surface integrity using the small area EDM process with a copper–tungsten electrode. *Mater. Sci. Eng. A* 364(1–2): 346–356. https://doi.org/10.1016/j.msea.2003.08.046

[31] Rahimi H, Masoudi S and Tolouei-Rad M 2022 Experimental investigation of the effect of EDM parameters and dielectric type on the surface integrity and topography. *Int. J. Adv. Manuf. Technol.* 118(5): 1767–1778. https://doi.org/10.1007/s00170-021-08040-z

[32] Lee H T and Liu C 2009 Optimizing the EDM hole-drilling strain gage method for the measurement of residual stress. *J. Mater. Process. Technol.* 209(15–16): 5626–5635. https://doi.org/10.1016/j.jmatprotec.2009.05.028

[33] Li L, Guo Y B, Wei X T and Li W 2013 Surface integrity characteristics in wire-EDM of Inconel 718 at different

discharge energy. *Proc. CirP* 6: 220–225. https://doi.org/10.1016/j.procir.2013.03.046

[34] Özerkan H B 2018 Simultaneous machining and surface alloying of AISI 1040 steel by electrical discharge machining with boron oxide powders. *J. Mech. Sci. Technol.* 32(9): 4357–4364. https://doi.org/10.1007/s12206-018-0834-0

[35] Wang F, Liu Y, Zhang Y, Tang Z, Ji R and Zheng C 2014 Compound machining of titanium alloy by super high speed EDM milling and arc machining. *J. Mater. Process. Technol.* 214(3): 531–538. https://doi.org/10.1016/j.jmatprotec.2013.10.015

[36] Lim L C, Lee L C, Wong Y S and Lu H H 1991 Solidification microstructure of electrodischarge machined surfaces of tool steels. *Mater. Sci. Technol.* 7(3): 239–248. https://doi.org/10.1179/mst.1991.7.3.239

[37] Jabbaripour B, Sadeghi M H, Faridvand S and Shabgard M R 2012 Investigating the effects of EDM parameters on surface integrity, MRR and TWR in machining of Ti–6Al–4V. *Mach. Sci. Technol.* 16(3): 419–444. https://doi.org/10.1080/10910344.2012.698971

[38] Kunieda M, Yoshida M and Taniguchi N 1997 Electrical discharge machining in gas. *CIRP Ann.* 46(1): 143–146. https://doi.org/10.1016/S0007-8506(07)60794-X

[39] Govindan P and Joshi S S 2012 Analysis of micro-cracks on machined surfaces in dry electrical discharge machining. *J. Manuf. Process.* 14(3): 277–288. https://doi.org/10.1016/j.jmapro.2012.05.003

[40] Kumar S S, Uthayakumar M, Kumaran S T, Varol T and Canakci A 2019 Investigating the surface integrity of aluminium based composites machined by EDM. *Defence Technol.* 15(3): 338–343. https://doi.org/10.1016/j.dt.2018.08.011

[41] Sivakumar K, Kumar P M, Amarkarthik A, Jegadheeswaran S and Shanmugaprakash R 2021 Empirical modeling of material removal rate and surface roughness of OHNS steel using Cu-TiB2Tool in EDM. *Mater. Today Proc.* 45: 2725–2729. https://doi.org/10.1016/j.matpr.2020.11.597

[42] Joshi S N and Pande S S 2010 Thermo-physical modeling of die-sinking EDM process. *J. Manuf. Process.* 12(1): 45–56. https://doi.org/10.1016/j.jmapro.2010.02.001

[43] Yadav V K, Kumar P and Dvivedi A 2019 Effect of tool rotation in near-dry EDM process on machining characteristics of HSS. *Mater. Manuf. Process.* 34(7): 779–790. https://doi.org/10.1080/10426914.2019.1605171

[44] Chattopadhyay K D, Verma S, Satsangi P S and Sharma P C 2009 Development of empirical model for different process parameters during rotary electrical discharge machining of copper–steel (EN-8) system. *J. Mater. Process. Technol.* 209(3): 1454–1465. https://doi.org/10.1016/j.jmatprotec.2008.03.068

[45] Senthilkumar V and Omprakash B U 2011 Effect of Titanium Carbide particle addition in the aluminium composite on EDM process parameters. *J. Manuf. Process.* 13(1): 60–66. https://doi.org/10.1016/j.jmapro.2010.10.005